

Polarization-Dependent Photoinduced Effects in Silicon-Doped Yttrium Iron Garnet

Richard Alben

Becton Center, Yale University, New Haven, Connecticut 06520
and

E. M. Gyorgy, J. F. Dillon, Jr., and J. P. Remeika
Bell Telephone Laboratories, Murray Hill, New Jersey, 07974

(Received 16 November 1971)

Polarization-dependent effects of light on the magnetic properties of silicon-doped yttrium iron garnet are described theoretically. The effects are identified with a process wherein photons selectively detach electrons from orientationally inequivalent Fe^{2+} centers. A crystal-field theory (including cubic-, trigonal-, and nontrigonal-distortion crystal fields) and spin-orbit coupling and exchange, is used to compute the wave functions for the different centers. The wave functions of the inequivalent centers present quite different cross sections to incoming photons of a given polarization. With some simplifying assumptions, we compute the anisotropy of the photodetachment cross sections. It is found that prolonged irradiation along the [110] direction, for example, can cause a 5 to 10% imbalance in the distribution of electrons among centers. The uniaxial anisotropy and dichroism associated with this imbalance are calculated and compared with our measurements. Our experiments are arranged so as to characterize the polarization-dependent photoinduced uniaxial anisotropy and distinguish it from other anisotropies. For example, we find that a uniaxial anisotropy energy $\mathcal{G}_u = -\gamma_1\gamma_2 \times (4.1 \pm 0.5) \times 10^3 \text{ erg cm}^{-3}$ is induced by polarization-dependent processes at 4.2°K in a sample in which 1% of the "d"-site Fe ions are replaced by Si. The experimental results can be explained by our theory in two ways. Either all Fe^{2+} centers contribute weakly to the effects or most centers are effectively inert and a few strong centers are responsible. These two alternatives are discussed in the light of previous observations of magnetic aftereffect and magnetic-resonance phenomena.

I. INTRODUCTION

Silicon-doped yttrium iron garnet (YIG: Si) is one of a small number of substances whose magnetic properties are easily changed when the material is irradiated with light.¹ The changes which occur during irradiation are called photomagnetic effects, or equivalently, photoinduced effects. Photoinduced changes in YIG: Si are more or less permanent as long as the material is kept at cryogenic temperatures.

For the purpose of this paper, two types of photoinduced effects are distinguished. The first type, whose discovery by Teale and Temple² opened the study of photomagnetism, is light-induced magnetic aftereffects³ or "photomagnetic anneal." In causing photomagnetic anneal, light acts like a high-temperature heat bath: It jostles active centers (which will be described presently) out of the sites at which they had been trapped and allows them to move about until they are trapped by other sites. The over-all change in the positions of the centers is determined by the trapping powers of the different types of sites. Since sites of lowest energy tend to be good traps, we can understand why photomagnetic anneal is in many ways similar to the thermally induced aftereffect.⁴⁻⁶

The second type of effect is that for which the vector character of the incident light governs the

direction in which magnetic properties are altered.⁹⁻¹³ These are polarization-dependent effects. In the case of polarization-dependent effects, light of a definite polarization interacts differently with centers trapped on different types of sites. In particular, certain sites are more likely to have centers detached by light than are other sites. We will assume that the polarization-dependent part of the over-all change in the positions of centers is determined by the detachment probabilities, or cross sections, of the different sites. Thus we distinguish two classes of effects and associate them with two fundamentally different mechanisms.

In this paper we will be dealing primarily with polarization-dependent effects. Below, in this section, we discuss the nature of the active centers in YIG: Si. In Sec. II, we describe an approximate but quantitative theory of photoinduced effects based on a photodetachment mechanism. In Sec. III, we apply the theory to the active centers in YIG: Si. We work out a crystal-field theory of the electronic states involved in the photodetachment process and calculate predictions for photodetachment cross sections associated with different sites and different polarizations for the incident light. We then obtain predictions for photoinduced uniaxial anisotropy and dichroism as a function of the crystal-field parameters used in the calculation. In Sec.

IV, we present measurements by which we have characterized photoinduced uniaxial anisotropy. The results are consistent with previous measurements but go much further in describing and separating the variations of the effects with the orientations of the light polarization and of the magnetization of the sample while it is being irradiated. We show that the experimental results for polarization-dependent-induced anisotropy can be explained by our photodetachment theory. We conclude in Sec. V with a discussion of the problem of quantitatively understanding all photoinduced effects in terms of a unified microscopic theory.

There have been several attempts to explain the photoinduced effects and also (thermal) magnetic aftereffects in YIG: Si in terms of a microscopic model of the active centers introduced by doping YIG with Si.^{14,15} It is generally agreed that Si is accommodated in tetrahedral ("d") sites in the YIG structure where it has an effective valence of 4⁺. Since the normal occupant of the d site is Fe³⁺, there must be one extra electron for each Si⁴⁺ in order to maintain over-all charge neutrality of the crystal. The extra electrons apparently are trapped on octahedral ("a") sites where they convert the normal Fe³⁺ occupants of the a sites to what we shall call Fe²⁺ centers. The symmetry of such effects as induced uniaxial anisotropy reflects that of the a site and provides some direct evidence that a-site Fe²⁺ centers are responsible for the photoinduced effects. In this picture then, a sites are traps for Fe²⁺ centers, and centers may move among the large number of available traps by the excitation and transfer of the extra electrons.

It is here that the agreement among authors regarding the active centers ends. The properties assigned to the Fe²⁺ centers have varied enormously,¹² depending on the effects to be explained. Recently, it has been proposed that the combined ef-

fects of different types of centers can qualitatively explain many photoinduced effects.¹⁵ Indeed, measurements of the photoinduced changes in absorptivity¹⁶ versus temperature clearly demonstrate that many kinds of Fe²⁺ centers exist in YIG: Si.

Although we cannot resolve the question of the origin of the variety of active centers, it is useful to briefly consider how different types of centers might arise. In pure YIG there are 16 types of a sites. They are said to be orientationally inequivalent since they differ only by spacial rotations. In YIG: Si, however, there are many types of sites which will be called chemically inequivalent in that they differ in the relative positions and/or types of defects or impurities in their vicinity. Centers on chemically inequivalent sites might have different crystal-field energies, thermal mobilities, activation energies, and magnetic anisotropy characteristics.

The most obvious impurities which might affect the a sites, and the only ones about which much can be said, are the Si⁴⁺'s. In Table I we present some quantities of interest in understanding what the effect a given Si⁴⁺ (located on a d site) might be on active centers located on a sites up to eighth-neighbor distance. The first two columns show the distances from the Si⁴⁺ and the number of neighbors at the given distance. The third column shows the relative energies of the ground states of different neighbors. One factor which distinguishes site energies is the electrostatic potential associated with the effective positive charge of the Si⁴⁺. This has been estimated by taking the static dielectric constant as 10.⁸ For the nearest-neighbor site, at least, we must recognize that the Si⁴⁺ may also influence the energy by creating a local distortion of the lattice. For example, Si⁴⁺ is expected to bind quite strongly to its surrounding oxygens; it might pull them closer to itself and cause a local

TABLE I. a-site neighbors of a reference d site. The characteristics of different a sites neighboring a d-site Si⁴⁺ center are shown. Except for the nearest-neighbor site, only the electrostatic effect of the Si⁴⁺ electron deficiency is included. For the nearest neighbor, a guess of the effect of the expected distortion of the site is shown. The dielectric constant has been taken as 10.

	Distance from d site (Å)	Number of a sites	Energy (cm ⁻¹)	Electric field (10 ⁶ V/cm)	Crystal field (D _x in cm ⁻¹)
1	3.44	4	-3387 ± 2000?	12.2	20 ± 100?
2	5.54	4	-2094	4.6	3
3	7.05	8	-1647	2.9	2
4	8.28	12	-1402	2.1	2
5	9.35	4	-1241	1.6	1
6	10.31	12	-1125	1.4	1
7	11.19	12	-1037	1.3	1
8	12.01	12	-966	1.0	0

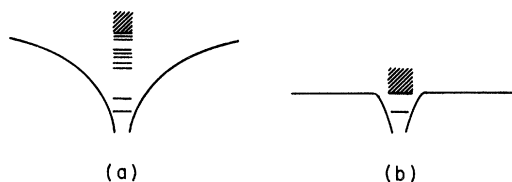


FIG. 1. Comparison of photoionization and photodetachment processes. The effective one-electron potential-energy curve and energy levels are shown for (a) a neutral atom in free space. When an electron of the atom is well outside the core it sees an attractive potential due to the net positive charge which it leaves behind. The region of attractive potential is quite extensive and there are many excited bound states. Photoionization occurs when light is absorbed and an electron is raised to a state in the ionization continuum (indicated by the diagonal stripes). Also shown is (b) a negative ion in free space. When an electron of the ion is beyond the core it sees no attraction at all. The effective potential well exists in only a small region and there are few if any bound excited states. Photodetachment occurs when light is absorbed and an electron is raised to the "detachment" continuum, leaving behind a neutral atom. In the text it is argued that an ion in a solid is analogous to a neutral atom if it has the proper valence for its site (e.g., Fe^{3+} on a sites in YIG). An ion with a lower valence is analogous to a negative ion (e.g., Fe^{2+} on a sites in YIG:Si).

buildup of negative, rather than positive, charge and so raise the energy of a nearest-neighbor center. This uncertainty is indicated in the table by the energy of $\pm 2000 \text{ cm}^{-1}$ followed by a question mark for the nearest-neighbor site.

If the energies shown in Table I are close to the real values, then all electrons with appreciable mobility at liquid-nitrogen temperature or below should find their way to nearest- or next-nearest-neighbor sites. It is also possible that some electrons might become frozen in higher energy, more distant sites, or that they might prefer a sites which neighbor some different type of impurity or defect, not a Si^{4+} . These possibilities make it difficult to draw definite conclusions regarding the distribution of centers among chemically inequivalent sites.

In the fourth column of Table I, we give the electric fields at the different sites. This is a measure of the forces tending to pull the centers toward lower-energy sites near the Si^{4+} . Finally, in the last column, we give an energy associated with the field gradient at each site. For the nearest neighbor we include an estimate of additional effects which might be associated with local distortions around the Si^{4+} : The energies are given in terms of the nontrigonal crystal field described in Sec. III. If these numbers are correct, then all sites except the nearest neighbor see only a negligibly small field gradient.

It is possible that the active centers are influenced

by impurities or defects other than Si^{4+} or by pairs of Si impurities. Little can be said regarding these possibilities except to note that the probability that pairs of Si impurities might influence a given site can be calculated if it is assumed that the Si ion substitutes randomly on d sites and if the doping level is known. The doping is usually denoted δ and is defined by a chemical formula for YIG: Si of the form $\text{Y}_3\text{Fe}_{5-\delta}\text{Si}_6\text{O}_{12}$. For the effects we discuss, δ is usually between 0.1 and 0.01. If $\delta = 0.1$, about 50% of the a sites which are first neighbors to an Si^{4+} impurity would have no other Si impurity closer than a fourth neighbor, while about 20% of such first-neighbor a sites would simultaneously be first neighbor to two Si^{4+} 's. Thus, for relevant values of δ , both fairly isolated and also highly perturbed a sites exist in YIG: Si.

From present knowledge, it is hopeless to attempt a unique characterization of the various sites possible for the Fe^{2+} centers. However, much can be learned from the following considerations of the behavior of a general model of the centers for a wide range of parameters.

II. PHOTODETACHMENT AS MECHANISM FOR PHOTO-INDUCED EFFECTS

Photodetachment is a word used to describe the process in which a photon is absorbed by a negative ion which then emits an electron and becomes a neutral atom.¹⁷ It is inappropriate to describe this process as photoionization since it results in an atom, not an ion. In this section we make an analogy between the interaction of light with Fe^{2+} centers in YIG: Si and the more usual processes of photodetachment. We will use that analogy in choosing approximations to treat that part of the light-induced redistribution of Fe^{2+} centers which depends on light polarization.

In Fig. 1 we show a schematic representation of a Hartree self-consistent potential for a free neutral atom and a free negative ion. For the neutral atom, the potential is attractive out to large distances from the core since any given electron will always see the net positive charge of the nucleus and the other electrons. Such a potential well generally should have many bound excited states associated with it; that is, there should be excited states for which all electrons are still localized in the vicinity of the core. Furthermore, the energy necessary to excite an electron into the continuum states, that is, the states for which an electron leaves the core completely, should be rather high. By contrast, the potential curve of the negative ion [see Fig. 1(b)] indicates that there is no attraction once a given electron gets outside the core. This potential well may not have any bound excited states. Also, the continuum states should lie relatively low in energy.

Now the Fe^{2+} center is like a negative ion in that it has one more electron than is normal for the site which it occupies. There are negative charges on the anions near the site which are arrayed in such a way that any given electron would see no net positive charge if it were removed from the immediate vicinity of the Fe core. Thus we should expect that an electron could be detached by a relatively low-energy photon. Furthermore, the states which describe the electron leaving the center should have something of the character of continuum states; that is, they should occur in a broad energy band with no really sharp structure, and they should not be characterized by a few definite quantum numbers. Rather, there should be many types of states lying at a rather low energy above the ground state. Each should be associated with a high probability that the excited electron will leave the site on which it was originally located.

There is some evidence regarding the energy distribution of the excited states of the Fe^{2+} centers: A broad peak about 4000 cm^{-1} wide centered at about $10\,000 \text{ cm}^{-1}$ has been seen in the absorption and photoinduced dichroism spectra of YIG: Si.¹³ We do *not* assign this structure to a parity-forbidden $d-d$ transition. Such transitions are seen for Fe^{2+} ions on sites for which $2+$ is the normal valence [e. g., $\text{Fe}(\text{H}_2\text{O}_6)^{2+}$ in aqueous solution¹⁸ and $\text{Fe}_3\text{Al}_2(\text{SiO}_4)_3$ ¹⁹]. However, the oscillator strengths of $d-d$ transitions²⁰ are far too low to account for the absorption seen in YIG: Si¹³ or for the rate at which photoinduced anisotropy is established²¹ by a given photon flux. In our picture of the Fe^{2+} center there are parity-allowed transitions to appropriate states in the continuum at the energies in question, and these account for the absorption. The observed structure may reflect properties of the continuum bands. We should note that the concept of photodetachment as we use it is only meant to be an approximate one. We do not need to assume that there will be a well-defined conduction band to represent our continuum states. Our arguments could also be expressed in terms of hopping or tunnelling of excited electrons away from a given center. The point is that with the assumption that a continuum of excited states takes part in photodetachment, some questions can be answered approximately without knowing much about excited states at all. Only the character of ground states of the electron on center will have to be considered.

The role of photodetachment in photoinduced effects is demonstrated by considering the rate of change, while the sample is being irradiated, of the numbers of Fe^{2+} centers located on the different a sites. We consider inequivalent sites i . The number of centers on the i th type of site is given by n_i . The n_i 's obey the following rate equation:

$$\frac{dn_i}{dt} = -In_i\sigma_i - \frac{n_i}{\tau_i} + rK_i \quad (1)$$

The first term summarizes the process of photodetachment; I is the light intensity; and σ_i is the photodetachment cross section, which is the effective target area seen by photons which may detach electrons trapped on the i th type of site. The second term represents processes where electrons spontaneously leave a given site due to thermal processes; τ_i is thus a thermal relaxation time.

The last term in (1) represents the trapping of excited electrons which can move among sites. It deserves special discussion here since it plays an important role in redistributing Fe^{2+} centers, but is not associated with what we have called photodetachment and will not be considered in detail in the rest of this paper. The flux of excited electrons is denoted r . It is the same for all inequivalent sites. The trapping cross section associated with this flux is K_i . This depends on the site specification i since different sites may have different ground-state energies for the electrons as well as other differences which affect their abilities to trap electrons. Specifically, ground states on different sites have energies which differ by anywhere from 5 to 100 cm^{-1} . The excited states presumably have energies equivalent to the photon energies of $10\,000 \text{ cm}^{-1}$. Even if the trapping process occurs by a direct deexcitation of the excited electrons, the energy differences could have a substantial effect on the abilities of the various sites to trap electrons. Furthermore, if the deexcitation occurs in a number of stages, the low-energy sites might be very favored traps indeed.

It turns out to be very difficult to do quantitative calculations about the variation of K_i with the type of site i . Thus in this paper we will neglect this variation. In doing so, we will fail to describe a class of processes which, in the Introduction, we have called photomagnetic anneal—the light-induced migration of Fe^{2+} centers to lower-energy sites. (We may also fail to describe some other processes as well.) Note, however, that K_i could not very easily depend on the polarization of the photon responsible for detaching the electrons. Thus little of the polarization-dependent effects should be lost by our neglect of the variation of K_i . In this sense then, by neglecting the variation of the trapping cross section K_i , we are concentrating on polarization-dependent effects whose origin must be in the variation of the detachment cross section σ_i with site index i , and with the polarization of the incoming photons.

Returning to (1), we note that in thermal equilibrium the left-hand term is zero. Then, the equilibrium numbers of Fe^{2+} centers on sites of type i are given by

$$n_i = \text{const} \times \frac{K_i}{\sigma_i + 1/\tau_i I}, \quad (2)$$

where const is some constant independent of i . This equation shows that sites with low detachment or high trapping cross sections tend to become populated with extra electrons at the expense of sites with high detachment and low trapping cross sections.

In Fig. 2 we show pictorially the nature of the dependence of the detachment cross section on the polarization of the incident photons. In case (a), a horizontally polarized photon is incident upon a wave function characterized by a charge density which resembles a pancake in the horizontal plane. The cross section is much higher than it is for case (b), where a vertically polarized photon is incident on the same wave function. Different behavior is illustrated by cases (c) and (d) for which the wave function resembles a vertically oriented cigar. We now describe a simple example which illustrates how the polarization dependence of σ_i leads to a photoinducible uniaxial anisotropy.

A cubic crystal is oriented so that the light polarization and any applied fields lie in the (001)

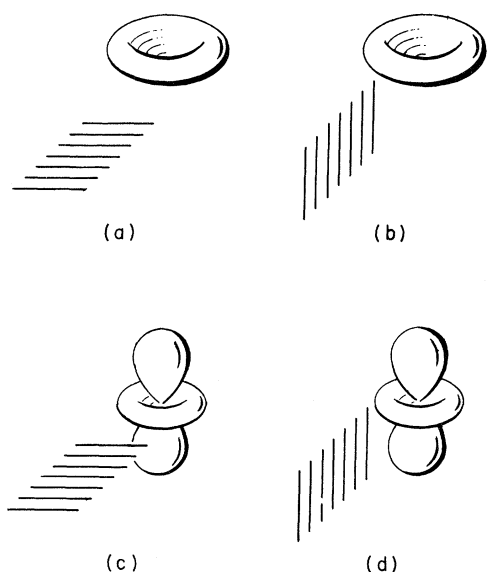


FIG. 2. Illustration of the dependence of the (averaged) photodetachment cross section on the shape of the initial orbital and the polarization of the incoming photon. The orbitals are d functions for which $m_l = 2$ [(a) and (b)] and $m_l = 0$ [(c) and (d)]. The shape of the orbitals is indicated by a surface which roughly delineates the region of high electron density. The incoming photon is represented by the parallel lines, the directions of which give the electric polarization of the photon. The relative values of the cross sections are case (a): 9; case (b): 3; case (c): 5; case (d): 11. [See the discussion leading to Eq. (14) for the approximations used to obtain the above results.]

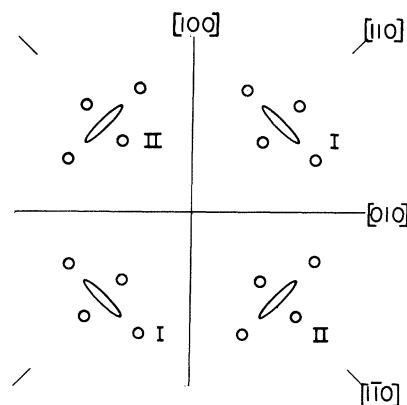


FIG. 3. Inequivalent sites in a simplified model of the (100) plane in a cubic crystal. The open circles represent the positions of the ligands which surround each site. The ellipses represent the distorted ground-state wave function of an electron located on the metal ion. The short axis of the ellipse is assumed to be the easy direction for the spin of the ion. For the two type-I sites the easy axis is $[110]$. For the two type-II sites it is $[1\bar{1}0]$.

plane (see Fig. 3). Associated with this plane are two types of sites which are orientationally inequivalent and of uniaxial symmetry. The unique axis, which corresponds to the z direction in local axes, is along the $[110]$ crystal direction for type-I sites and along $[1\bar{1}0]$ for type II. We assume that σ has been calculated and found to be of the axially symmetric form:

$$\sigma = \sigma_0 [1 + B(1 - 2(\hat{\alpha}_i)_z^2)], \quad (3)$$

where $\hat{\alpha}_i$ is the light polarization direction in the local axes of site i and the caret of $\hat{\alpha}_i$ denotes a unit vector. The average absolute cross section σ_0 and the relative anisotropy in the cross section B are constants derived by considering the nature of the ground-state wave function of the trapped electron. (We will compute constants such as σ_0 and B for YIG: Si in Sec. III.) Similarly, the energy associated with a trapped electron is assumed to have been calculated and to have the axially symmetric form (again in local axes)

$$E_i = E_0 + P[1 - 2(\hat{\gamma}_i)_z^2], \quad (4)$$

where $\hat{\gamma}_i$ is the magnetization direction (in local coordinates) of the site i , and P is a uniaxial anisotropy constant computed from the ground-state wave function. (The meanings of $\hat{\alpha}$, $\hat{\gamma}$, and also another direction to be described later are shown in Fig. 4.) Finally, we neglect any variation of K_i with i , and take τ_i very long so that thermal relaxation can be neglected.

Now with $\hat{\alpha}$ expressed in the axes of the crystal, the values of σ for the two types of sites differ.

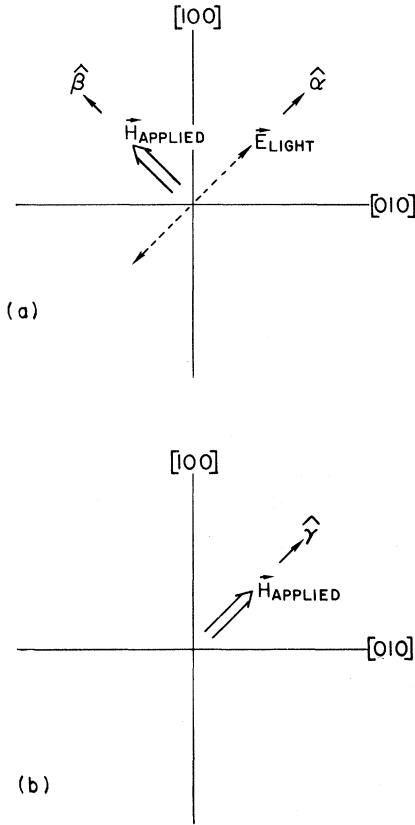


FIG. 4. Definition of the directions $\hat{\alpha}$, $\hat{\beta}$, and $\hat{\gamma}$. (a) During treatment with light, the moment of the sample is held (by an applied field $H_{APPLIED}$) in direction $\hat{\beta}$. The light polarization E_{LIGHT} is parallel to $\hat{\alpha}$. (b) After treatment the torque is measured. The direction of the moment during measurement is $\hat{\gamma}$. The anisotropy after treatment is described by the energy as a function of $\hat{\gamma}$.

From (3) we find

$$\sigma_I = \sigma_0[1 - 2B\alpha_1\alpha_2], \quad \sigma_{II} = \sigma_0[1 + 2B\alpha_1\alpha_2]. \quad (5)$$

From (5) and (2) we obtain the difference in the number of centers on the two types of sites in equilibrium during irradiation:

$$n_I - n_{II} = 2B\alpha_1\alpha_2n, \quad (6)$$

where we have assumed that n , the total number of centers, is conserved.

We may note from (5) and (6) that sites with the lower detachment cross section tend to become populated. Clearly, a variation in the trapping cross sections would affect this result in such a way as to favor sites with higher trapping cross sections while isotropic thermal relaxation would generally reduce population imbalances.

The total energy after the population difference (6) is established follows from (4) by weighting the energy contribution from each site by its popula-

tion. Thus we have

$$\mathcal{E} = \sum_i n_i E_i, \quad (7)$$

where

$$E_I = E_0 - 2P\gamma_1\gamma_2, \quad E_{II} = E_0 + 2P\gamma_1\gamma_2, \quad (8)$$

and

$$\mathcal{E} = n(E_0 - 4PB\alpha_1\alpha_2\gamma_1\gamma_2). \quad (9)$$

The angular-dependent part of the energy represents a uniaxial anisotropy for which either $[110]$ or $[1\bar{1}0]$ is the easy axis. Its magnitude is the product of the anisotropy in the detachment cross section and the intrinsic single-site uniaxial anisotropy. It is notable that, with the approximations used, the saturation value of the induced population difference involves only the relative anisotropy in the cross section. The absolute cross section enters most directly in measurements of dichroism.

The photoinduced dichroism is found by considering the absolute cross section associated with each type of site weighted by the n_i 's. Thus the absorptivity for light polarized along $\hat{\alpha}'$ is

$$\mu = \mu_0 - 4n\sigma_0B^2\alpha_1'\alpha_2'\alpha_1\alpha_2, \quad (10)$$

where μ_0 is a direction-independent term and $\hat{\alpha}'$ is, as before, the direction of the light polarization used to establish the population imbalance. The magnitude of the dichroism varies as the square of the relative anisotropy in the cross section, is independent of the magnetic anisotropy, and is scaled by the absolute cross section.

Although the simple example discussed above does not apply directly to YIG: Si, the differences are all due to the complexity of site geometry and the multiplicity of different sites expected in YIG: Si. The general principles and physical approximations described in this section will all be used in more detailed calculations which follow.

III. CALCULATION OF PHOTOINDUCED EFFECTS IN YIG: Si

A. Introduction

In this section we present a crystal-field calculation for the photodetachment cross sections and magnetic energies for the orientationally inequivalent "a" sites in YIG: Si. From these results we compute predictions for the photoinduced uniaxial anisotropy and dichroism. As far as possible, we present quantitative predictions taking due note of the assumptions which we make in order to complete the calculations.

B. Wave Functions and Energies

We treat the Fe^{2+} center in the crystal-field approximation. That is, the ground-state wave function is constructed from d orbitals of what is es-

essentially a free Fe^{2+} ion influenced by electrostatic fields associated with the crystalline environment. This approximation has well-known drawbacks¹⁸ which might be quite severe in the case we consider where one of the Fe^{2+} electrons is very weakly bound. If experience in related calculations^{22,23} is taken as a guide, we should expect that properties which are sensitive to the radial dependence of the wave function may be badly estimated by crystal-field theory. Properties relating to the symmetry of the wave function should be better estimated.

The free Fe^{2+} ion has the configuration $[\text{Ar}](3d)^6$. The electronic ground state is 5D which is best pictured as one added d electron outside of a half-filled d shell. The half-filled shell couples strongly to the spin of the added electron, but the symmetry of the orbital part of the many-electron wave function is just that of the added electron's d orbital. Photodetachment presumably involves changing the orbital of the added electron.

The effects of the YIG: Si a -site environment on an Fe^{2+} ion are summarized by the following Hamiltonian:

$$H = B_4(O_4^0 - 20\sqrt{3}O_4^3) - 71\vec{L} \cdot \vec{S} - 600\hat{m} \cdot \vec{S} - D_z(3L_z^2 - 6) + D_x(3L_x^2 - 6) \text{ (cm}^{-1}\text{)}, \quad (11)$$

where \vec{L} refers to the $l=2$ D manifold, \hat{m} is the magnetization direction, and \vec{S} is the spin ($s=2$) of the 5D multiplet. The first term on the right-hand side is a cubic-crystal-field energy expressed in trigonal axes. The O 's are tensor operators. We take B_4 to be very large and positive (the usual sign for sixfold oxygen coordination) so that only the 15-state $^5T_{2g}$ submultiplet of 5D needs to be considered. The second term represents spin-orbit coupling, somewhat reduced from the free-ion value, as is usual for ions in crystals. The third term is an isotropic exchange of the same magnitude experienced by the a -site Fe^{3+} ion in YIG²⁴; \hat{m} is the direction of the net moment of the material. Of course, this term can only be considered to be a rough estimate of the form and magnitude of the exchange associated with the Fe^{2+} wave function; but it should give the general features of the effect of the net moment on the shape and the energy of the Fe^{2+} wave function.

The fourth term in (11) is the trigonal-crystal-field energy which originates with the trigonal distortion of the octahedron of oxygen ions surrounding the a site; z corresponds to $[111]$, $[\bar{1}11]$, $[1\bar{1}1]$, or $[11\bar{1}]$, depending on the particular a site being described. The value of D_z cannot be computed and is treated as an adjustable parameter. Considering the behavior of YIG: Si, it is reasonable to consider only positive values of D_z so that the local z axis is an easy direction for spin. The order of magnitude of D_z should be about 200 cm^{-1} .

The last term in (11) is the nontrigonal-crystal-field energy. This destroys the C_{3i} symmetry of the problem and provides a means of quenching the orbital angular momentum left by the trigonal field. From a strictly practical point of view, this parameter is necessary to control (that is, to reduce) the magnetic anisotropy for the purpose of fitting experimental results. Physically, a symmetry-lowering field might be caused by Si^{4+} ions in the neighborhood of the Fe^{2+} center. The magnitude of D_x would be 20 cm^{-1} if the effect were due to the field gradient of a charge deficiency on a nearest-neighbor d site as noted earlier (see Table I). D_x should be much smaller for more distant sites. We will treat D_x as an adjustable parameter and consider values up to $100\text{--}300 \text{ cm}^{-1}$. The higher values are considered since they correspond to one possible experimental fit. However, it is not easy to imagine how such high values of D_x might come about. Without appreciable loss of generality, we can take D_x positive, so that x tends to be a hard direction for the spin. It should be noted that the orientation of the local x axis, associated with the nontrigonal field, is not of much consequence since the over-all site symmetry is so low (C_1) that principal axes appropriate to various effects are not directly related to the geometry of the site.

In a sense, we are doing a model calculation; we do not really know the parameters appropriate to YIG: Si Fe^{2+} centers. Thus we wish to keep things as simple as possible, while still preserving the essence of the problem. An extremely important feature of YIG: Si is its over-all cubic symmetry. In order for this to be maintained, there must be at least three symmetrically related directions for the x axis associated with each of the four directions for the local z axis. We consider then the minimum number of 12 differently oriented Fe^{2+} centers. The directions of the 12 sets of local-site axes in the cubic coordinates are given in Table II. Except for considerations of cubic symmetry, the local x axis directions were chosen arbitrarily.²⁵

In actual materials, there are, no doubt, far more than 12 orientationally inequivalent sites. Indeed, there are probably several types of chemically inequivalent sites which contribute to the photoinduced effects; but even with just 12 sites our calculation requires fairly complicated geometry in its interpretation. Thus we reserve comment on these added complications present in real crystals until after our basic 12-site-model calculation is described.

We have diagonalized the Hamiltonian (11) for a range of values of D_z and D_x and with various directions for \hat{m} . We obtained the ground-state energies and the angular-dependent parts of the ground-state wave functions for each of the twelve

TABLE II. Directions in cubic axes of the x , y , and z local axes for each of the 12 orientationally inequivalent a sites considered in the model calculation.

Site label	Directions of local axes		
	x	y	z
1	[11 $\bar{2}$]	[$\bar{1}$ 10]	[111]
2	[$\bar{1}$ 1 $\bar{2}$]	[$\bar{1}$ $\bar{1}$ 0]	[$\bar{1}$ 11]
3	[$\bar{1}\bar{1}\bar{2}$]	[1 $\bar{1}$ 0]	[$\bar{1}\bar{1}$ 1]
4	[11 $\bar{2}$]	[110]	[$\bar{1}\bar{1}$ 1]
5	[$\bar{2}$ 11]	[0 $\bar{1}$ 1]	[111]
6	[$\bar{1}\bar{2}$ 1]	[101]	[$\bar{1}$ 11]
7	[$\bar{2}$ 11]	[011]	[$\bar{1}\bar{1}$ 1]
8	[121]	[$\bar{1}$ 01]	[$\bar{1}\bar{1}$ 1]
9	[1 $\bar{2}$ 1]	[10 $\bar{1}$]	[111]
10	[211]	[01 $\bar{1}$]	[$\bar{1}$ 11]
11	[$\bar{1}$ 21]	[$\bar{1}$ 0 $\bar{1}$]	[$\bar{1}\bar{1}$ 1]
12	[$\bar{2}$ 11]	[0 $\bar{1}\bar{1}$]	[$\bar{1}\bar{1}$ 1]

sites. The next step, which we now describe, is to compute the polarization-dependent photodetachment cross section associated with each wave function.

C. Photodetachment Cross Section

The general formula for the cross section for electric-dipole excitation from an initial orbital i to a final orbital f is²⁶

$$\sigma_{i,f} = (4\pi e^2/\lambda)A|\langle i|\vec{r}\cdot\hat{\alpha}|f\rangle|^2\rho(\hbar\omega) \quad , \quad (12)$$

where e is the electronic charge, λ and $\hat{\alpha}$ are the wavelength and polarization of the incident photons, A is a dimensionless factor of order unity which relates the optical electric field at the ion to the photon flux, and $\rho(\hbar\omega)$ is the density of final states at an energy $\hbar\omega$ (the photon energy) above the initial state. The computation of $\sigma_{i,f}$, in general, requires knowledge of the wave functions of the initial and final states. However, if our picture of photodetachment is valid, it is reasonable to assume that a number of excited states can contribute as final states in photodetachment. We may then consider an averaged excitation cross section which is much easier to estimate than parts referring to specific states.

For example, let us assume for purposes of illustration that all final states contribute equally. The average total cross section $\bar{\sigma}$ involves a sum over all final states. The result is

$$\bar{\sigma} = (4\pi e^2/\lambda\Delta E)A\hat{\alpha}\cdot\langle i|\vec{r}: \vec{r}|i\rangle\cdot\hat{\alpha} \quad , \quad (13)$$

where $1/\Delta E$ is the average density of states. This result involves only the initial orbital. When the initial orbital originates from a d -type wave function, the matrix element in (13) can be expressed

in terms of the (dimensionless) orbital angular-momentum \vec{L} as follows:

$$\langle i|\vec{r}: \vec{r}|i\rangle = \langle r^2\rangle/21 \langle i|7\vec{L} - 2(\vec{L}: \vec{L} - 2\vec{I})|i\rangle \quad , \quad (14)$$

where $\langle r^2\rangle$ is the ground-state expectation value of the square of the radial coordinate and \vec{I} is the unit diadic. The form of (14) implies that $\bar{\sigma}$ can be a rather strong function of the orientation of the photon polarization with respect to the initial-state wave function. Some extreme cases have already been illustrated in Fig. 2.

In considering photodetachment in YIG:Si, it is useful to distinguish two contributions to electric-dipole excitations, one from p -type final states, and one from f -type final states. (The dipole-moment operator \vec{r} links d orbitals to p and f angular-momentum orbitals.) By explicit consideration of the sums of matrix elements involved in the two contributions, we find the following expression for the total averaged cross section:

$$\bar{\sigma} = \hat{\alpha}\cdot[B_{dp}\langle 2\vec{I} - (\vec{L}: \vec{L} - 2\vec{I})\rangle + B_{df}\langle 7\vec{I} - (\vec{L}: \vec{L} - 2\vec{I})\rangle]\cdot\hat{\alpha} \quad , \quad (15)$$

where $\langle \rangle$ denotes ground-state expectation value, and

$$B_{dp} = \frac{4\pi e^2}{\lambda\Delta E} \frac{A}{15} \sum_{n_p} |\langle i|r|n_p\rangle|^2 \quad , \quad (16)$$

$$B_{df} = \frac{4\pi e}{\lambda\Delta E} \frac{A}{35} \sum_{n_f} |\langle i|r|n_f\rangle|^2 \quad , \quad (17)$$

where the sums run over all excited orbitals of the given angular momentum n_p for p states, n_f for f states. Note that if, indeed, all excited orbitals are included, then we may use the completeness of the radial wave functions belonging to each angular momentum to reduce the sums in (16) and (17) to $\langle r^2\rangle$. That would effectively recover (14).

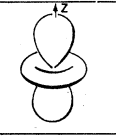
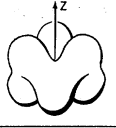
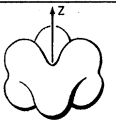
For Fe^{2+} , the $2p$ and $3p$ orbitals are lower in energy than the initial d orbital, are filled with electrons, and so must certainly be excluded from possible final states. We calculated the Fe^{2+} free-ion wave function using the Thomas-Fermi-Dirac method (Herman-Skillman program).²⁷ This method should be adequate since we only need to compute for inner shells of the ground-state configuration. The results of the calculations show that the filled states represent a substantial reduction for p -type contributions to $\langle r^2\rangle$. Explicitly, the full sum such as occurs in (17) yields

$$\sum_{n_f} |\langle i|r|n_f\rangle|^2 = \langle r^2\rangle = 1.4 \text{ (a. u.)}^2 \quad . \quad (18)$$

The sum in (16) is

$$\sum_{n_p \neq 2,3} |\langle i|r|n_p\rangle|^2 = 0.6 \text{ (a. u.)}^2 \quad . \quad (19)$$

TABLE III. Averaged photodetachment cross sections for t_{2g} orbitals. The trigonal axis is the axis of quantization z . The pictures in the second column show the shape of each orbital. σ_{hk} is the photodetachment cross section for light polarized along h . The constants B_{df} and B_{dp} are amplitudes of processes involving the f - and p -type angular-momentum states for the detached electron.

ORBITAL	CROSS SECTION	
	σ_{zz} \updownarrow	σ_{xx} \leftrightarrow
$t_{2g}^0 =$ Y_2^0 	$9B_{df} + 4B_{dp}$	$6B_{df} + B_{dp}$
$t_{2g}^+ =$ $\sqrt{\frac{2}{3}}Y_2^+ - \sqrt{\frac{1}{3}}Y_1^+$ 	$6B_{df} + B_{dp}$	$7\frac{1}{2}B_{df} + 2\frac{1}{2}B_{dp}$
$t_{2g}^- =$ $\sqrt{\frac{2}{3}}Y_2^- - \sqrt{\frac{1}{3}}Y_1^-$ 	$6B_{df} + B_{dp}$	$7\frac{1}{2}B_{df} + 2\frac{1}{2}B_{dp}$

In the interest of simplicity, we will neglect the somewhat reduced contributions from p -type excited states. Since the p -type excitation cross section is more anisotropic than that of the f -type processes, we will therefore tend to underestimate the anisotropy in the photodetachment cross section.

One further simplification of the cross-section calculation can be made by noting that the initial d -orbital for the a site contains only t_{2g} states. In terms of the effective angular momentum $l=1$ (referred to cubic, not local, axes) of the t_{2g} triplet, we have

$$\sigma = B_{df} \hat{\alpha} \cdot \langle 7 \vec{I} + (6 \sum_{k=x,y,z} \hat{n}_k I_k^2 \hat{n}_k - 3 \vec{I} \cdot \vec{I} - 2 \vec{I}) \rangle \cdot \hat{\alpha}, \quad (20)$$

where \hat{n}_k is a unit vector in the k direction. Note that the form of (20) reflects the loss of rotational symmetry due to the cubic crystal field. The variation of σ with $\hat{\alpha}$ is illustrated in Table III for several examples of initial orbitals. Note that, as before (Fig. 2), σ is greatest when the polarization corresponds to a long dimension of the wave function. In our calculations for YIG:Si, the initial wave functions are not those used in the table, but those found by diagonalizing the Hamiltonian (11). The behavior of the detachment cross section, however, is generally similar to that shown in Table III.

Thus far we have discussed the relative varia-

tion in σ which depends on the symmetry of the wave function. The absolute magnitude is given by the constant B_{df} . This has the units of area and is basically the physical cross section of the atom scaled by a coupling factor to the photon field. If in (16) and (17) we take $\Delta E = 1$ eV, $\langle r^2 \rangle$ from the Herman-Skillman calculation and the photon energy as 1 eV, we find that $B_{df} = 3 \times 10^{-19}$ cm². Since the average value of the expectation value in (20) is 7, the average cross section should be about 2×10^{-18} cm². The absorptivity μ associated with 2×10^{20} Fe²⁺/cm³ (corresponding to $\delta = 0.05$) would then be 400 cm⁻¹, which is in agreement with the results of Ref. 13. The considerations involved in this estimate are, of course, quite approximate. It is significant, however, that our photodetachment mechanism is of the correct order of magnitude to explain the absorptivity of YIG:Si (see also Ref. 21).

D. Calculation of Photoinduced Anisotropy and Dichroism from Photodetachment Cross Section

The photodetachment cross sections of the inequivalent sites in YIG:Si partially determine the numbers of Fe²⁺ centers on different a sites after the sample has been treated with light. From (2) we obtain

$$n_i = \sigma_i^{-1} / \sum_i \sigma_i^{-1}, \quad (21)$$

where we assume that all sites are equally good at trapping electrons and neglect thermal relaxation. The σ_i 's (and hence the n_i 's) depend on the light polarization direction and also on the direction of the moment of the sample during irradiation $\hat{\beta}$ as indicated in Fig. 4(a). We assume that no changes in the n_i 's occur after irradiation has ceased. After treatment, the material may be measured to determine such properties as anisotropy and dichroism. The direction of the magnetization during measurement is denoted $\hat{\gamma}$ [see Fig. 4(b)].

We consider first the induced uniaxial anisotropy. The uniaxial anisotropy energy \mathcal{E}_u of a crystal of YIG:Si with $\hat{\gamma}$ constrained to lie in the (001) plane is described by the following expression:

$$\mathcal{E}_u = -\gamma_1 \gamma_2 \bar{E}^C - \frac{1}{2} (\gamma_1^2 - \gamma_2^2) \bar{E}^D, \quad (22)$$

where \bar{E}^C refers to anisotropy associated with a [110] axis and \bar{E}^D refers to anisotropy associated with a [100] axis. (In Sec. II, only \bar{E}^C was considered.) We next define a set of quantities E_i^C and E_i^D which measure the contributions of individual Fe²⁺ centers of the sites i to the over-all magnetocrystalline anisotropy of the sample. The \bar{E} 's depend on the n 's and E_i 's as follows:

$$\bar{E}^{C,D} = \sum_i E_i^{C,D} n_i(\hat{\alpha}, \hat{\beta}), \quad (23)$$

TABLE IV. Test of validity of the truncated form for the photoinduced uniaxial anisotropy energy [Eq. (27)]. Here $\hat{\alpha}$ is taken as [210] and $\hat{\beta}$ is also taken as [210]. For each crystal field, \bar{E}^C and \bar{E}^D were computed from Eq. (23) (first results), and compared with the values implied by Eq. (27) (second results, in parentheses). Particularly for cases of large D_X , it is clear that Eq. (27) is adequate.

Crystal fields (cm ⁻¹)		Induced anisotropy (erg cm ⁻³)	
D_Z	D_X	\bar{E}^C ($\times 10^3$)	\bar{E}^D ($\times 10^3$)
200	0	275.0 (418.1)	0.0 (0.0)
200	10	252.0 (269.6)	1.96 (-5.40)
200	100	68.1 (69.2)	-13.56 (-13.75)

where we have indicated that n_i 's depend on $\hat{\alpha}$ and $\hat{\beta}$, but that the E_i 's do not depend on the past treatment of the sample. In our calculation we determined the E_i 's by considering numerical results for the ground-state energies, $W_i[\hat{m}]$ of each of the 12 differently oriented sites when the direction \hat{m} (which corresponds to $\hat{\gamma}$ in this case) was along [110], [1 $\bar{1}$ 0], [100], and [010] crystal directions. The E_i 's were identified as follows:

$$E_i^C = W_i[1\bar{1}0] - W_i[110], \quad E_i^D = W_i[010] - W_i[100]. \quad (24)$$

Using (21), (23), and (24), we could compute the \bar{E} 's for any given values of $\hat{\alpha}$ and $\hat{\beta}$.

For many cases the dependence of the \bar{E} 's on $\hat{\alpha}$ and $\hat{\beta}$ can be well approximated by the following forms, which are the simplest allowed by the symmetry of the (001) plane:

$$\bar{E}^C = C^\alpha \alpha_1 \alpha_2 + C^\beta \beta_1 \beta_2, \quad (25)$$

TABLE V. Calculated values for the photoinduced anisotropy and dichroism for different crystal fields; comparison with experiment. The C coefficients refer to uniaxial anisotropy along the [110] directions. The crystal fields D_X and D_Z are parameters in the local-site Hamiltonian [Eq. (11)]. The population differences refer to the difference in the numbers of Fe²⁺ centers on different classes of orientationally inequivalent a sites after treatment. For definitions of C^α and C^β , refer to Eq. (27); for $\Delta\mu^C$, see Eq. (29). The extrapolated experimental values for the C 's are discussed in Sec. IV B; those for the $\Delta\mu$'s are from Ref. 13. The sample doping corresponds to $\delta=0.03$. The temperature is taken as 4.2°K.

Crystal fields (cm ⁻¹)		$\left(\frac{n_I - n_{II}}{n}\right)10^{-3}$	C^α (10 ³ erg cm ⁻³)	C^β (10 ³ erg cm ⁻³)	$\Delta\mu^C$
D_Z	D_X				Average μ (10 ⁻²)
50	0	4.56	179.0	154.0	0.5
50	100	4.80	19.3	2.4	3.5
200	0	6.51	337.0	185.0	1.0
200	10	6.60	312.0	24.0	3.5
200	300	5.32	8.4	0.1	4.0
Experiment		...	20.0	70.0	0.6

(extrapolated to saturation)

$$E^D = D^\alpha \left[\frac{1}{2} (\alpha_1^2 - \alpha_2^2) \right] + D^\beta \left[\frac{1}{2} (\beta_1^2 - \beta_2^2) \right]. \quad (26)$$

With these forms for the \bar{E} 's, (22) becomes

$$\mathcal{G}_u = -\gamma_1 \gamma_2 (C^\alpha \alpha_1 \alpha_2 + C^\beta \beta_1 \beta_2) - \frac{1}{2} \gamma_1^2 \left\{ D^\alpha \left[\frac{1}{2} (\alpha_1^2 - \alpha_2^2) \right] + D^\beta \left[\frac{1}{2} (\beta_1^2 - \beta_2^2) \right] \right\}. \quad (27)$$

In the following, the form (27) will be assumed to be adequate to describe the theoretical results. In order to fix the C 's and D 's, it is sufficient to use (23) to evaluate the \bar{E} 's for two sets of directions of $\hat{\alpha}$ and $\hat{\beta}$ and to fit (25) and (26) to the results. We used the sets $\hat{\alpha} = [100]$, $\hat{\beta} = [110]$ and $\hat{\alpha} = [110]$, $\hat{\beta} = [100]$. We also checked results for other sets of $\hat{\alpha}$ and $\hat{\beta}$. As may be seen in Table IV, the approximate form is quite good, especially when D_X is large. (When D_X is small, there are "near crossings" involving the ground-state energy levels and these lead to large terms which are high order in $\hat{\beta}$.)

The dichroism is calculated quite analogously to the anisotropy. Consider first the absorptivity $\mu(\hat{\alpha}')$ of the material (after treatment) to light polarized along $\hat{\alpha}'$:

$$\mu(\hat{\alpha}') = \sum_i \sigma_i(\hat{\alpha}', \hat{\gamma}) n_i(\hat{\alpha}, \hat{\beta}), \quad (28)$$

where $\hat{\alpha}$, $\hat{\beta}$, and $\hat{\gamma}$ are used as before. We consider two types of dichroism $\Delta\mu^C$ and $\Delta\mu^D$:

$$\Delta\mu^C = \mu(1\bar{1}0) - \mu(110), \quad (29)$$

where $\hat{\alpha}$ is [110] and $\hat{\beta}$ and $\hat{\gamma}$ are [100], and

$$\Delta\mu^D = \mu(010) - \mu(100), \quad (30)$$

where $\hat{\alpha}$ is [100] and $\hat{\beta}$ and $\hat{\gamma}$ are [110].

E. Results of Calculations

The results of our calculation for anisotropy and dichroism are summarized in Tables V and VI.

We have taken the total number of contributing Fe^{2+} centers to correspond to a doping $\delta=0.03$. This is the doping (from optical absorption) of the sample used for our experiments. Where possible, we have included experimental results (from Sec. IV and Ref. 13) for comparison with the theory. Calculated results for five representative crystal-field parameters are shown. The crystal fields are given in the first column. In the second column, we give the population imbalances among orientationally inequivalent sites which can be created by irradiation. For effects associated with the [110] axis (Table V), the imbalance is calculated by adding the n_i 's of sites 1, 3, 5, 7, 9, and 11 (for which [110] is an easier direction than $[\bar{1}\bar{1}0]$, type I), subtracting the n_i 's of sites 2, 4, 6, 8, 10, and 12 (for which [110] is harder than $[\bar{1}\bar{1}0]$, type II), and dividing by n . The n_i 's are those corresponding to treatment with $\hat{\alpha}$ along [110] and $\hat{\beta}$ along [100]. For effects associated with the [100] axis (Table VI), the imbalance is gotten by adding the n_i 's of sites 6, 8, 9, and 11 (for which [100] is easier than [010], type I), subtracting the n_i 's of sites 5, 7, 10, and 12 (for which [100] is harder than [010], type II), and dividing by n . For this case, the n_i 's correspond to $\hat{\alpha}$ along [100] and $\hat{\beta}$ along [010].

In the third column of Table V, we show calculated results for C^α . This coefficient measures the [110] anisotropy induced by irradiating with light polarized along [110] while the magnetization is held along [100]. The calculated results warrant some special discussion since the trends are large enough to be insensitive to certain cancellations from different types of sites; and, also because the value derived from the photodetachment mechanism should account for most of the observed effect.

The most obvious trend is that C^α tends to be reduced by the presence of large nontrigonal crystal fields. This happens because the anisotropy

energy of each site is reduced as the nontrigonal field quenches the effective angular momentum. Note that the induced population imbalance is fairly insensitive to the nontrigonal crystal field since the wave function remains quite anisotropic in shape even as the angular momentum is quenched. Another significant fact is that C^α is calculated to be always positive; that is, light of a given polarization tends to depopulate most strongly those sites for which the polarization direction is a hard direction for the moment. This trend can be explained by the following rough argument: The magnetocrystalline anisotropy for the orbital singlet ground state is governed by the orbital angular momentum which can be induced by the spin moment via the spin-orbit coupling $\vec{L} \cdot \vec{S}$. If all excited states contribute equally to the induced moment, then for S along some axis z' , the anisotropy energy will be $-\lambda^2 S^2 \langle L_{z'}^2 \rangle / E_{ex}$, where E_{ex} is an average energy for excited states. For Fe^{2+} , $\langle L_{z'}^2 \rangle$ is largest when z' is roughly perpendicular to the plane on which the wave function makes its maximum projection. If this plane is fixed by crystal fields, then the easy direction for the spin is perpendicular to the plane, and hard directions are in the plane. But we have seen that the cross section for photodetachment is greatest when the light polarization is in the plane of the wave function. Therefore, as originally asserted, light will tend to depopulate sites for which the polarization direction is hard, and thus tend to make the polarization direction into an easy axis.

In the fourth column of Table V, we give results for C^β , which measures the anisotropy along [110] induced when $\hat{\alpha}$ is along [100] and $\hat{\beta}$ is along [110]. That is, C^β measures that we have called "photomagnetic anneal." The photodetachment mechanism can contribute somewhat to this effect because the exchange field can distort the orbital part of the wave

TABLE VI. Calculated values for the photoinduced anisotropy and dichroism for different crystal fields; comparison with experiment. The D coefficients refer to uniaxial anisotropy along the [100] direction. The crystal fields D_X and D_Z are parameters in the local-site Hamiltonian [Eq. (11)]. The population differences refer to the difference in the numbers of Fe^{2+} centers on different classes of orientationally inequivalent a sites after treatment. For definitions of D^α and D^β , refer to Eq. (27); for $\Delta\mu^D$, see Eq. (30). The extrapolated experimental values for the D 's are discussed in Sec. IV B; those for $\Delta\mu^D$ are from Ref. 13. The sample doping corresponds to $\delta=0.03$. The temperature is taken as 4.2 °K.

Crystal fields (cm^{-1})		$\left(\frac{n_{\text{I}'} - n_{\text{II}'}}{n}\right) 10^{-2}$	D^α (10^3 erg cm^{-3})	D^β (10^3 erg cm^{-3})	$\Delta\mu^D$ Average μ (10^{-2})
D_Z	D_X				
50	0	0.00	0.0	0.0	0.00
50	100	0.20	1.9	-1.5	0.01
200	0	0.00	0.0	0.0	0.00
200	10	2.02	-9.0	-0.1	0.80
200	300	0.63	-2.1	-0.1	0.10
Experiment		...	1.2	5.6	0.10

(extrapolated to saturation)

TABLE VII. Contributions to the photoinduced anisotropy coefficient C^α from each of the 12 orientationally inequivalent sites. In this example $D_z = 50 \text{ cm}^{-1}$ and $D_x = 100 \text{ cm}^{-1}$. The E_i 's give the contribution of an Fe^{2+} on the site of type i . The σ_i 's (given for $\hat{\alpha}$ along [110] and $\hat{\beta}$ along [100]) determine the numbers of Fe^{2+} 's on each type of site. The magnetic energy after irradiation is given by Eqs. (22) and (23). The result is $\delta_\mu = -0.385 \times \gamma_1 \gamma_2 \text{ cm}^{-1}$ per Fe^{2+} .

Site label i	E_i^c (cm^{-1})	σ_i (Relative units)	$(n_i/n - \frac{1}{12})10^{-2}$
1 and 3	22.0	7.870	-1.06
5 and 7	14.6	6.005	+1.20
9 and 11	14.6	6.091	+1.06
2 and 4	-22.0	6.083	+1.08
6 and 8	-14.6	7.919	-1.11
10 and 12	-14.6	7.988	-1.17

function through the spin-orbit coupling. The effect is greatly weakened even by moderate nontrigonal crystal fields because the wave function tends to become pinned, in a sense, by the crystal fields. As discussed in Sec. I, there is a large contribution to photomagnetic anneal expected from mechanisms other than photodetachment. Thus it is not surprising that the size of C^α relative to C^β , calculated from the photodetachment mechanism alone, is much smaller than the experimental results indicate it should be.

In the third and fourth columns of Table VI we present results for D^α and D^β . These coefficients would be zero were it not for the nontrigonal crystal field which associates each inequivalent site with [100]-type directions as well as with [111]-type directions. In the cases where the nontrigonal field is large, the D 's turn out to be of the order of 10% of the corresponding C 's in our calculation. However, there is some cancellation involved in this model which suppresses the D 's somewhat more than might be expected. Note that the D 's change sign in several cases.

The structure of the results for photoinduced anisotropy is more fully illustrated in Table VII. Here we consider the contributions to C^α for the case $D_z = 50$, $D_x = 100$. In the first column are the labels of the different inequivalent sites. In the second column, we give the contribution that an Fe^{2+} center located on the given sites makes to the over-all uniaxial anisotropy along [110]. The third column gives the photodetachment cross section of an Fe^{2+} for each site when $\hat{\alpha} = [110]$ and $\hat{\beta} = [100]$. Note that for sites 1 and 3 and 2 and 4 the "rule" that sites tend to have small cross sections for light polarized along their easy axis is violated. An explanation for this may be seen from Table II. Recall that in local axes, z is an easy direction while x is a hard direction. The wave function tends to be

elongated along x and flattened perpendicular to z . Now consider site 1. The wave function is quite elongated along x which corresponds to the crystal $[11\bar{2}]$ direction. Thus, for this site, x has a substantial projection on the [110] direction, the direction of $\hat{\alpha}$. When all the effects of the cubic crystal field and spin-orbit coupling are added in, this site does have a substantial cross section even though [110] is a relatively easy direction. Similar competing effects account for the anomalous behavior of sites 2, 3, and 4.²⁸

In the fourth column of Table VII we give the excess populations caused by irradiation. Considering (23) and (27), for the given $\hat{\alpha}$ and $\hat{\beta}$ we may identify

$$C^\alpha = 2 \sum_i E_i^c n_i = 0.770 \text{ cm}^{-1}/\text{Fe}^{2+} \\ = 19.3 \times 10^3 \text{ erg cm}^{-3}, \quad \delta = 0.03 \quad (31)$$

Returning to the fifth columns of Tables V and VI, we consider the fractional photoinduced dichroism [Eqs. (29) and (30)]. Note that the dichroism tends to increase with the nontrigonal field, in direct contrast to the results for the inducible anisotropy. The disparity in behavior of these two effects is due first to the fact that the dichroism depends on population imbalances only and not on the magnetic anisotropy of the individual sites. Second, the squares of the anisotropy in the cross section contribute to dichroism [see Eq. (10)] so there is no cancellation from differently behaving sites.

It is to be noted that the results of Tables V and VI apply for situations where only a single chemical type of a site is allowed to contribute. If several chemically different types of sites with different crystal fields were simultaneously present, the results would not simply be averaged. Rather, the expected population distribution among sites would have to be considered in detail. This point will be discussed further in Sec. V after we present our experimental results.

IV. EXPERIMENTAL MEASUREMENTS OF PHOTOINDUCED UNIAXIAL ANISOTROPY; COMPARISON WITH THEORY

A. Experimental Measurements

We now describe new experimental measurements which enable us to characterize the dependence of the photoinduced uniaxial anisotropy on the light polarization and the direction of magnetization during irradiation. The experimental results are then compared, insofar as it is possible, with the theoretical predictions of Sec. III.

Our experiments differ in two important respects from previous work^{9,12} on photoinduced anisotropy in YIG:Si. First, we perform our measurements with polarization and magnetization in the (001) plane. This simple plane contains most of the im-

portant information regarding directional-dependent behavior in a cubic material while its high symmetry allows measurements to be easily interpreted and classified. Second, we handle, in a somewhat novel fashion, the problem of subtracting off effects due to anisotropy annealed in prior to irradiation. We cool the sample from room temperature to 4.2 °K with the moment held along a principal crystallographic direction ([100] or [110]). After the appropriate treatment we measure the torque with the moment along this same direction. Insofar as we could properly align the sample, the torque is a measure of the absolute anisotropy induced during treatment. By making our measurements only of torque changes, we avoid the uncertainties introduced by crystalline and shape anisotropies as well as anisotropies induced by cooling, which would have made a direct measurement of the absolute anisotropy quite difficult to interpret.

In contrast, in the pioneering work of Pearson *et al.*,⁹ anisotropy induced prior to treatment was eliminated by irradiating for a very long time. The absolute size of the induced anisotropy was found by Fourier analysis of the torque curves. However, since there are many types of spurious anisotropies, and also relaxation effects, present in that type of measurement, we believe our method of carefully analyzing the torque developed at one angle to be a superior method of measurement for the case at hand.

In earlier work by three of us¹² results relating to the effect of irradiation on samples cooled in general crystallographic directions were reported. However, it was difficult to interpret the effects be-

cause of the anisotropy induced during cooling. We now consider the measurements reported below, for which the sample was cooled so as to establish a constant reference state before treatment, to be of the most interest.

Our sample was an (001) disk of YIG:Si for which δ was 0.03, as determined by optical absorption. We made measurements at both liquid-nitrogen²⁹ and liquid-helium temperatures, but only the helium results, which were less subject to relaxation effects, will be reported here.

Each run consisted of four steps: (i) warm to room temperature to erase the effects of previous treatment; (ii) cool to liquid-helium temperature with the magnetization in either the [100] or the [110] direction; (iii) rotate the magnetization to a predetermined direction (generally different for each run) and irradiate for 50 sec with light of an intensity of 0.370 W/cm² and a polarization direction $\hat{\alpha}$ (this about half-saturated the induced effects); (iv) return the field to its initial position and measure the change in torque. The above procedure could be accomplished in a short time—measurement commenced about 5 sec after the end of irradiation—and so transients were not a serious problem. By judiciously choosing directions of field and polarization, we were able to separately determine the magnitudes of the various constants (discussed below) that describe the induced anisotropy and are allowed by symmetry. We also made numerous checks on our results.

We present the results in terms of the following expression for the uniaxial anisotropy energy of a sample which has been treated with light:

$$\begin{aligned} \mathcal{E}_u = & -\gamma_1\gamma_2 \left[C^\alpha \alpha_1 \alpha_2 + C^\beta \beta_1 \beta_2 + 4C^{\alpha\beta} \left(\frac{\beta_1^2 - \beta_2^2}{2} \right)^2 \alpha_1 \alpha_2 + 4C^{\beta\alpha} \frac{\beta_1^2 - \beta_2^2}{2} \frac{\alpha_1^2 - \alpha_2^2}{2} \beta_1 \beta_2 + 4C^{\beta\beta} \left(\frac{\beta_1^2 - \beta_2^2}{2} \right)^2 \beta_1 \beta_2 \right] \\ & - \frac{\gamma_1^2 - \gamma_2^2}{2} \left[D^\alpha \frac{\alpha_1^2 - \alpha_2^2}{2} + D^\beta \frac{\beta_1^2 - \beta_2^2}{2} + 4D^{\alpha\beta} (\beta_1 \beta_2)^2 \frac{\alpha_1^2 - \alpha_2^2}{2} + 4D^{\beta\alpha} \beta_1 \beta_2 \alpha_1 \alpha_2 \frac{\beta_1^2 - \beta_2^2}{2} + 4D^{\beta\beta} \frac{\beta_1^2 - \beta_2^2}{2} (\beta_1 \beta_2)^2 \right], \end{aligned} \quad (32)$$

where $\hat{\alpha}$, $\hat{\beta}$, and $\hat{\gamma}$ are used as before (see Fig. 2). The form of (32) is motivated by the irreducible representations of the C_4 symmetry group appropriate to the (001) plane. We have included (i) no terms higher than second order in $\hat{\alpha}$, since the effects vary as the light intensity and thus as the square of the optical electric field; (ii) only terms second order in $\hat{\gamma}$ since only these correspond to a uniaxial anisotropy; and (iii) no terms higher than eighth order in all direction cosines, a natural limit to the complexity worth considering. If we had considered arbitrary directions with terms up to eighth order in $\hat{\alpha}$, $\hat{\beta}$, and $\hat{\gamma}$, 17 terms would have occurred, where all the added terms are of sixth and eighth order.

It should be noted that the eighth-order terms in (32) were quite apparent in our measurements. The use of only the fourth-order terms [as in Eq. (27)] would have led to an uncertainty of over 50% in the value of C^α , for example.

From (32) we find the torque when $\hat{\gamma}$ is along [100], T_{100} , is given by

$$\begin{aligned} T_{100} = & C^\alpha \alpha_1 \alpha_2 + C^\beta \beta_1 \beta_2 + 4C^{\alpha\beta} \left(\frac{\beta_1^2 - \beta_2^2}{2} \right)^2 \alpha_1 \alpha_2 \\ & + 4C^{\beta\alpha} \frac{\beta_1^2 - \beta_2^2}{2} \frac{\alpha_1^2 - \alpha_2^2}{2} \beta_1 \beta_2 \\ & + 4C^{\beta\beta} \left(\frac{\beta_1^2 - \beta_2^2}{2} \right)^2 \beta_1 \beta_2, \end{aligned} \quad (33)$$

where positive torque corresponds to a tendency

TABLE VIII. Summary of experimental results for photoinduced anisotropy in the (001) plane. Induced anisotropy coefficients for 50-sec irradiation, and 25 sec after the start of measurement are given. For significance of the various coefficients see Eq. (32). The doping is $\delta = 0.03$ and the temperature is 4.2 °K.

Photoinduced anisotropy coefficients (erg cm ⁻³)	
(10 ³)	(10 ³)
$C^\alpha = 10.2 \pm 2.0$	$D^\alpha = 0.6 \pm 1.0$
$C^{\alpha\beta} = 6.2 \pm 2.0$	$D^{\alpha\beta} = 0.4 \pm 1.0$
$C^\beta = 34.8 \pm 2.0$	$D^\beta = 2.8 \pm 1.0$
$C_{\text{dark}}^\beta = 6.8 \pm 2.0$	$D_{\text{dark}}^\beta = 0 \pm 1.0$
$C^{\beta\beta} = 16.8 \pm 10$	$D^{\beta\beta} = 1.0 \pm 6.0$
$C^{\beta\alpha} = 0.0 \pm 4.0$	$D^{\beta\alpha} = 1.2 \pm 2.0$

of the crystal to rotate so that the [100] direction moves toward [010]. The torque with $\hat{\gamma}$ along [110], T_{110} , is given by

$$T_{110} = - \left[D^\alpha \frac{\alpha_1^2 - \alpha_2^2}{2} + D^\beta \frac{\beta_1^2 - \beta_2^2}{2} + 4D^{\alpha\beta} \left(\frac{\alpha_1^2 - \alpha_2^2}{2} \right) (\beta_1 \beta_2)^2 + 4D^{\beta\alpha} \beta_1 \beta_2 \alpha_1 \alpha_2 \frac{\beta_1^2 - \beta_2^2}{2} + 4D^{\beta\beta} \frac{\beta_1^2 - \beta_2^2}{2} (\beta_1 \beta_2)^2 \right]. \quad (34)$$

We measured T_{100} and T_{110} for various values of α and β and found that the results could be fitted if the C 's and D 's were given the values shown in Table VIII.

We discuss the significance of our results by considering certain of the combinations of $\hat{\alpha}$'s and $\hat{\beta}$'s which could be used to determine each of the coefficients. We will only consider the C 's in detail since the D 's are related to the corresponding C 's by a 45° rotation. For all the C 's, the sample is cooled with the moment along [100].

To measure C^α and C^β we first illuminate the sample [Step (iii)] with $\hat{\alpha}$ along [110] and $\hat{\beta}$ along [110]. The moment is returned to [100] and the torque recorded as in the upper curve of Fig. 5. Note that over a period of several minutes the induced torque relaxes to about 75% of its original value. In the next run, the illumination is performed with $\hat{\alpha}$ along [110] and $\hat{\beta}$ along [110]. The lower curve in Fig. 5 shows the result. Examination of (33) shows the first curve to be $\frac{1}{2}(C^\beta + C^\alpha)$ and the second to be $\frac{1}{2}(-C^\beta + C^\alpha)$. The vector sum and the difference of the two results yield C^α and C^β as functions of time. Averaging a number of determinations of this sort, we find that at 25 sec after the measurement begins $C^\alpha = (10.2 \pm 2.0) \times 10^3$ erg cm⁻³ and $C^\beta = (34.8 \pm 2.0) \times 10^3$ erg cm⁻³. Parenthetically, we remark that due to a calibration error the corresponding values given in Table II of Ref. 29 should be doubled.

The coefficient C^β also may be measured by a

quite different procedure which should be equivalent if (32) is an adequate expression. This involves an irradiation step with $\hat{\alpha}$ along [100] and $\hat{\beta}$ along [110]. The measured torque multiplied by 2 is then C^β . This approach does, in fact, give the same result as that of the preceding paragraph. There is a contribution to C^β , denoted C_{dark}^β , which is measured by running with $\hat{\beta}$ along [110] with no illumination during the 50-sec treatment period. This represents a purely thermal annealing effect and, as shown in Table VIII, is substantial even at these low temperatures.

Consider next $C^{\alpha\beta}$. This can be determined from a run with $\hat{\alpha}$ along [110] and $\hat{\beta}$ along [100]. From (33) we see that twice the measured torque should be $C^\alpha + C^{\alpha\beta}$. In this way we find that $C^{\alpha\beta}$ is 6.2×10^3 erg cm⁻³. Obviously, if $C^{\alpha\beta}$ were assumed to be zero, as in (27), a considerable discrepancy would occur in attempting to reconcile the results of this run with those described above. The origin of $C^{\alpha\beta}$ is in a saturation effect. That is, if the induced torque is plotted against $\hat{\beta}$ with $\hat{\alpha}$ always along [110], it is seen that the curve bends over the torque associated with the $\hat{\alpha}$ and $\hat{\beta}$ directions come to reinforce each other. The term $C^{\beta\beta}$ is measured by taking $\hat{\alpha}$ along [100] and plotting the induced torque as a function of $\hat{\beta}$. A saturation effect is seen in that the maximum in the torque, which occurs near $\hat{\beta} = [110]$, is very flat. A similar effect is known for thermally induced anisotropy.¹² The last coefficient $C^{\beta\alpha}$ is also measured by taking $\hat{\alpha}$ along [100] and plotting the induced torque against $\hat{\beta}$. With $\hat{\alpha}$ along [100], the (110) plane no longer has fourfold symmetry, and this could be manifested in a lack of fourfold symmetry in variation of torque with $\hat{\beta}$. It turns out, however, that $C^{\beta\alpha}$ is essentially zero.

The most striking feature of the results for the D 's is that they are a factor of 10 or so smaller than the C 's. This result is well known from previous work,⁹ and presumably is a manifestation of the fact that the principal directions of the local-site uniaxial anisotropies are approximately along [111]-type axes.

We can, to some extent, compare our results with those of Pearson *et al.*⁹ They studied the rather complicated (110) plane and, with their data, it is not possible to characterize their sample as extensively as we have done with ours. If we neglect all coefficients except for C^α and C^β , then the uniaxial energy appropriate to the (110) is

$$\mathcal{E}_u = -\gamma_1 \gamma_2 (C^\alpha \alpha_a \alpha_b + C^\beta \beta_a \beta_b) - \frac{\gamma_a^2}{2} \left(C^\alpha \frac{\alpha_a^2}{4} + C^\beta \frac{\beta_a^2}{4} \right), \quad (35)$$

where a and b refer to the [110] and the [001] axes, respectively. Fitting this to the results of Ref. 9, we find

$$C^\alpha = 6.4 \times 10^3 \text{ erg cm}^{-3}, \quad C^\beta = 10 \times 10^3 \text{ erg cm}^{-3} \quad (36)$$

These values may be compared with those in Table VIII. The sample used in the experiments of Ref. 9 was nominally of the same composition as ours, and, within the large uncertainty caused by the neglect of higher coefficients and sample effects, there is substantial agreement.

We conclude this part with an illustration of the over-all effect of treatment on the free energy of a sample of YIG: Si. Figure 6(a) shows a polar plot of the free energy as a function of $\hat{\gamma}$ for the (001) plane of a hypothetical sample for which all orientationally inequivalent sites are equally populated (see Ref. 8). This should be roughly appropriate for a doping $\delta = 0.03$ at 4.2°K . Note that, in contrast to the situation in pure YIG, the rather substantial fourfold anisotropy is of such a sign (at this temperature) so that [100]-type directions are

easy. Figure 6(b) shows the free energy after cooling with the moment along [100]. There is some adjustment of the n_i 's, and [100] becomes an easier direction than [010]. There is no torque developed, however. In Fig. 6(c) we show the effect of irradiation with $\hat{\alpha}$ along [110] while $\hat{\beta}$ is along [100]. It is seen that the easy direction shifts by about 10° from [100].

B. Comparison with Calculations

In comparing the experimental results with our calculation we must account for the fact that we did not saturate the photoinduced anisotropy in our experiments. It is reasonable to take the equilibrium C 's and D 's as twice the experimental results. This is what we have done in Tables V and VI.

Consider first C^β . We have noted earlier that the exchange field does not disturb the wave function strongly enough for the photodetachment mechan-

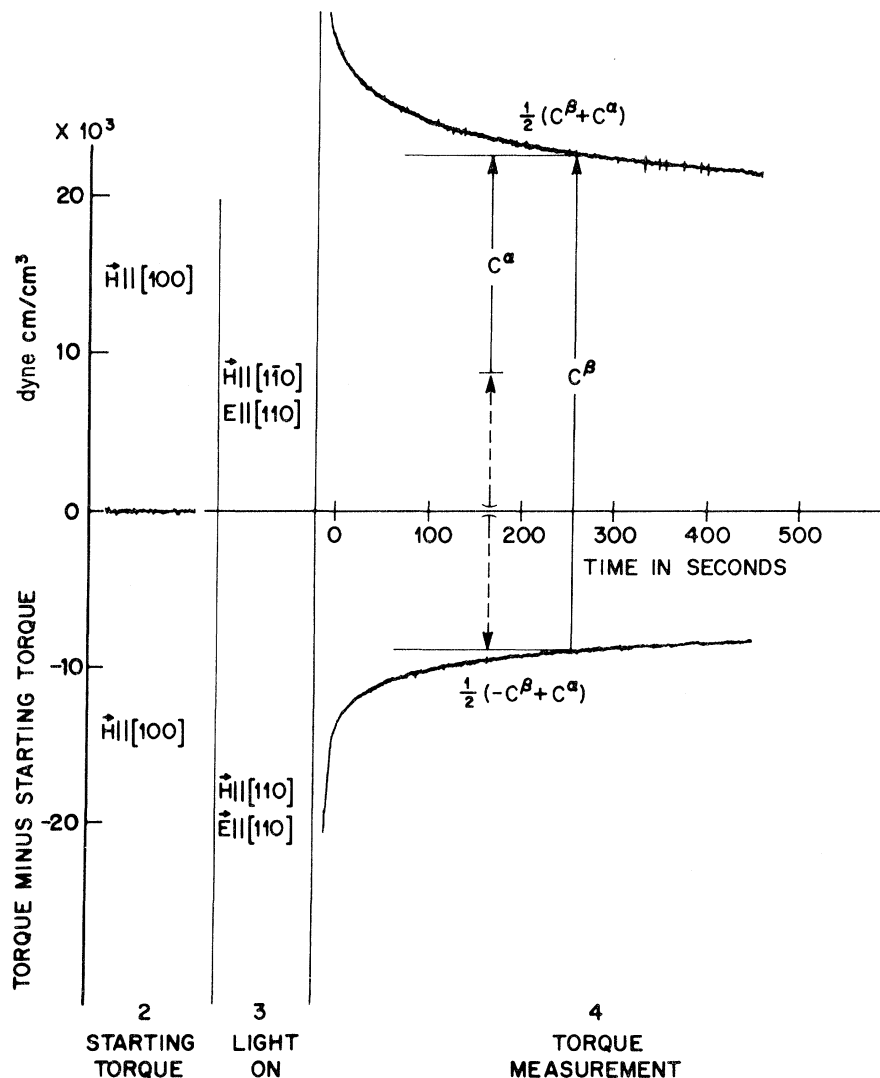


FIG. 5. Illustration of procedure used to characterize the photoinduced uniaxial anisotropy. The torque measured for two different runs is shown. The difference in the torques for these runs can be identified with the coefficient C^β in Eq. (32). Their vector sum is C^α .

ism to be used to account for the relatively large observed value of C^β . It appears that a large contribution to C^β is coming from properties of the process by which a sites trap electrons. This process is probably responsible also for the higher-order C coefficients as well.

Thus we are left with C^α as the most significant coefficient which can be explained by the photodetachment-model calculation. There are two ways of reconciling the small observed size of this co-

efficient with the values associated with various parametrizations of the model. First we might assume that the active sites are associated with very large nontrigonal crystal fields ($D_x \sim 300 \text{ cm}^{-1}$) which suppress the intrinsic uniaxial anisotropy of each site. While this explanation should not be ruled out, it is hard to understand the origin of the nontrigonal field required.

A second explanation is that only a few sites with relatively small trigonal distortions contribute strongly to the effects, while most Fe^{2+} centers are on sites which are unable to contribute. The inert Fe^{2+} sites could be accounted for if there were a number of chemically inequivalent sites. Some of these might not contribute to induced anisotropy because the electrons could easily tunnel to similar sites of different orientation, thereby relaxing away all induced population imbalances in a short time. Some sites might not contribute because the electrons were so very strongly trapped that they could not respond to treatment by light. A deeper understanding of the distribution of Fe^{2+} ions among inequivalent sites will be required before the implications of this second explanation can be evaluated.

V. ON A MODEL INCLUDING ALL SPECIAL EFFECTS FOUND IN YIG:Si

We have concluded that polarization-dependent photoinduced effects in YIG:Si can be explained by photodetachment of electrons from Fe^{2+} centers. We now relate our detailed model of the centers to others which have been proposed to explain observations regarding magnetic aftereffect,^{6,7} resonance,^{8,9,30} permeability,^{3,15} and absorption^{13,16} in YIG:Si. We shall see that there are some real problems in reconciling these effects and the different models which have been used to explain them.

First we consider the class of thermal after-effects (annealing) and rotational hysteresis. These have been explained^{6,7} on the basis of a model in which the Fe^{2+} centers are described by a magnetic anisotropy energy of the form

$$E_1 = -\epsilon \cos^2 \theta_i, \quad (37)$$

where θ_i is the angle between the magnetization and trigonal-distortion axis appropriate to the i th site. The anisotropy which results from thermal anneal depends on ϵ and also on the temperatures at which electrons become permanently trapped on the various inequivalent a sites. Various values of ϵ have been proposed. van Groenou^{7,31} mentioned a value $\epsilon = 1 \text{ cm}^{-1}$ which seems to be too low since he took a single relaxation time in getting this result. Hunt⁶ took a value of $\epsilon = 5 \text{ cm}^{-1}$, which does reproduce the magnitude of the observed anisotropy if a number of Fe^{2+} centers equal to the nominal

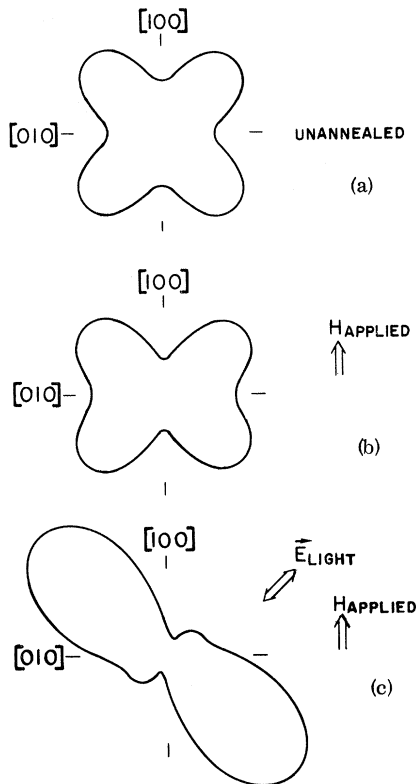


FIG. 6. Illustration of the effects of a particular combination of thermal and light treatment on the free energy of YIG:Si ($\delta=0.03$). The free energy is plotted in polar coordinates. The angle corresponds to the direction $\hat{\gamma}$ of the moment in the (001) plane, and the radius gives the free energy. Data on samples of quite different dopings were used in obtaining the results shown; they can only be regarded as approximate. (a) Free energy after cooling in a rapidly rotating field (equal distribution of Fe^{2+} 's among differently oriented sites). The [100]-type directions are easy. The free energy E is $E = K_1 \gamma_1^2 \gamma_2^2$, where $K_1 = 1.2 \times 10^4 \text{ erg cm}^{-3}$ (deduced indirectly from Ref. 6, Fig. 18). (b) Free energy after cooling with the moment along [100]. The [100] direction becomes somewhat easier than [010]. $E = K_1 \gamma_1^2 \gamma_2^2 - K_U^D [\frac{1}{2}(\gamma_1^2 - \gamma_2^2)]$, where $K_U^D = +2000 \text{ erg cm}^{-3}$ (from Ref. 6). (c) Free energy after irradiation with $\hat{\alpha}$ along [110], $\hat{\beta}$ along [100]. The easy direction rotates by 10° and a large torque would now be required to hold the moment along [100]. $E = K_1 \gamma_1^2 \gamma_2^2 - K_U^D [\frac{1}{2}(\gamma_1^2 - \gamma_2^2)] \frac{1}{2} C^\alpha \gamma_1 \gamma_2$, where $C^\alpha = 10^4 \text{ erg cm}^{-3}$ (from Tables V and VI).

TABLE IX. Thermally induced magnetic anisotropy for various crystal fields at 4.2°K. The annealing temperature is taken as 25°K. Anisotropy associated with the [100] axis generally is small and has been neglected. The doping is taken as $\delta = 0.03$.

$\delta_u = -G^C \gamma_1 \gamma_2 \beta_1 \beta_2$ (erg cm ⁻³)		G^C ($\delta = 0.03$) (10 ³)
Crystals fields (cm ⁻¹)		
D_z	D_x	
50	0	3760
50	10	3610
50	50	1520
50	100	440
50	200	80
200	0	5010
200	20	3890
200	50	2300
200	100	880
200	200	170
(Experiment—Refs. 6 and 8)		50–80

Si doping are assumed to contribute. We have calculated the annealed anisotropy implied by our 12-site model for various crystal fields and obtained the results shown in Table IX. For these results, the numbers of Fe²⁺ centers on the different sites were found by assuming that an equilibrium was established at 25°K. The crystal field values are not directly related to the ϵ parameter of (37) but considering the variation of energy levels with \hat{m} , we may say that $D_z = 50$ cm⁻¹, $D_x = 200$ cm⁻¹ roughly corresponds to $\epsilon = 10$ cm⁻¹. The results in Table IX then substantially confirm that the ϵ value used by Hunt can explain the annealed effects with all Fe²⁺s contributing. However, the nontrigonal crystal field which corresponds to this ϵ ($D_x = 300$ cm⁻¹) is very large indeed. Another difficulty with this model occurs in explaining the angular variation of the annealable anisotropy (see Ref. 12).

The effect of Si doping on the field for magnetic resonance⁸ has been explained with a very different model than that described above. Here the equivalent of ϵ is taken to be about 70 cm⁻¹ and departures from the form (37) are essential to explain the behavior of the field for resonance along the [100] direction. Only about one-fifth of the spectroscopically determined doping is assumed to contribute to this essentially nonannealable effect, and a far smaller fraction of sites is allowed to participate in effects involving redistribution of Fe²⁺ centers among sites. The problem here is

to understand what happens to the ineffective Fe²⁺s.

Very striking effects of light on the permeability and absorption have been seen in very lightly doped samples ($\delta < 0.01$).¹⁶ Since the effects decrease above this doping, it may be surmised that sites more than 30 Å from any Si⁴⁺ are necessary for them to occur. Perhaps among these sites which are relatively far from impurities only those very far sites can trap electrons and so become stable Fe²⁺ centers. In any case, such far sites do not exist in materials doped strongly enough to display the polarization-dependent induced anisotropy. However, one fact relevant to the case at hand which is pointed up by these results on lightly doped samples¹⁶ is that a large number of chemically inequivalent centers do exist in YIG: Si.

Finally, we return to the polarization-dependent photoinduced effects analyzed in this paper. The uncertainty of our theory is sufficiently great that many sites weakly contributing or few sites strongly contributing can form the basis of an explanation of the photoinduced anisotropy. However, the predicted photoinduced dichroism, which is not nearly as sensitive to the crystal-field values, is considerably larger than that observed. This is an indication then that some, perhaps most, sites are not contributing to this photoinduced effect, and this favors the second explanation.

In conclusion, we see that models of very different character can be used to explain, with varying success, various effects seen in YIG: Si. Until we have achieved a better understanding of the nature of the different kinds of active centers which result from Si substitution, it does not seem possible to decide which model, or combination of models, is really the most appropriate. In any case, it does appear that the anisotropic shape of the wave function of the highest-energy orbital of Fe²⁺ ions on *a* sites can be used, with a photodetachment mechanism, to explain the polarization-dependent photoinduced anisotropy and dichroism which have been measured in YIG: Si.

ACKNOWLEDGMENTS

The authors acknowledge with thanks the invaluable technical assistance of E. Heilner in taking the torque data, E. M. Kelly in the growth of the single crystals, and C. R. Staton in the preparation of the samples. The authors are especially grateful to Miss E. Prescott for many measurements of optical absorption.

¹Other photomagnetic materials include Ga-doped cadmium chromium selenide [W. Lems, P. J. Rijnierse, P. F. Bongers, and U. Enz, Phys. Rev. Letters **21**, 1643 (1968)], ferric borate [D. E. Lacklison, J. Chadwick and J. L. Page, J. Appl. Phys. **42**, 1445 (1971)],

and Co-doped nickel zinc ferrite [Th. Holtwijk, W. Lems, A. Verhulst, and U. Enz, IEEE Trans. Magnetics (to be published)].

²R. W. Teale and D. W. Temple, Phys. Rev. Letters **19**, 904 (1967).

- ³U. Enz and H. van der Heide, *Solid State Commun.* **5**, 347 (1968).
- ⁴R. L. Comstock and C. E. Fay, *J. Appl. Phys.* **36**, 1253 (1965).
- ⁵D. J. Epstein and L. Toici, *Appl. Phys. Letters* **11**, 55 (1967).
- ⁶R. P. Hunt, *J. Appl. Phys.* **38**, 2826 (1967).
- ⁷A. Broese van Groenou, J. L. Page, and R. F. Pearson, *J. Phys. Chem. Solids* **28**, 1017 (1967).
- ⁸T. S. Hartwick and J. Smit, *J. Appl. Phys.* **40**, 3995 (1969).
- ⁹R. F. Pearson, A. D. Annis, and P. Kompfner, *Phys. Rev. Letters* **21**, 1805 (1968).
- ¹⁰J. F. Dillon, Jr., E. M. Gyorgy, and J. P. Remeika, *Phys. Rev. Letters* **22**, 643 (1969).
- ¹¹J. F. Dillon, Jr., E. M. Gyorgy, and J. F. Remeika, *Appl. Phys. Letters* **15**, 221 (1969).
- ¹²E. M. Gyorgy, J. F. Dillon, Jr., and J. P. Remeika, *IBM J. Res. Develop.* **14**, 321 (1970).
- ¹³J. F. Dillon, Jr., E. M. Gyorgy, and J. P. Remeika, *J. Appl. Phys.* **41**, 1211 (1970).
- ¹⁴R. W. Teale and D. W. Temple, U. Enz, and R. F. Pearson, *J. Appl. Phys.* **40**, 1435 (1969).
- ¹⁵U. Enz, R. Metselaar, and P. J. Rijnierse, *J. Phys. (Paris) Suppl.* **32**, C1-703 (1971).
- ¹⁶J. F. Dillon, Jr., E. M. Gyorgy, and J. P. Remeika, *J. Phys. (Paris) Suppl.* **32**, C1-794 (1971); E. M. Gyorgy, J. R. Dillon, Jr., and J. P. Remeika, *J. Appl. Phys.* **42**, 1454 (1971).
- ¹⁷See, for example, review by L. M. Branscomb, in *Atomic and Molecular Processes*, edited by D. R. Bates (Academic, New York, 1962), p. 100.
- ¹⁸See C. J. Ballhausen, *Introduction to Ligand Field Theory* (McGraw-Hill, New York, 1962), p. 252.
- ¹⁹P. Bloomfield, A. W. Lawson, and Charles Rey, *J. Chem. Phys.* **34**, 749 (1961).
- ²⁰See J. S. Griffith, *The Theory of Transition-Metal Ions* (Cambridge U. P., London, 1964), p. 288.
- ²¹The time t associated with inducing an anisotropy is $1/I\sigma$, where I is the photon flux and σ is the detachment cross section. For our experiment I was 10^{16} – 10^{17} photons/sec over most of the sample. Taking t as 50 sec, we find that σ must be of the order of 10^{-18} cm². This corresponds to an oscillator strength of about 10^{-2} .
- ²²B. R. Judd, *Phys. Rev.* **127**, 750 (1962).
- ²³G. S. Ofelt, *J. Chem. Phys.* **37**, 511 (1962).
- ²⁴R. Gonano, E. Hunt, and H. Meyer, *Phys. Rev.* **156**, 521 (1967).
- ²⁵It might be noted in passing that nearest-neighbor d sites (possible locations for Si⁴⁺ ion) may be found along [102], [210], and [021] axes centered on some of the a sites for which [111] is the trigonal axis. Little would be gained from the added complication of associating non-trigonal crystal fields with each of these many types of axes.
- ²⁶See, for example, W. Heitler, *The Quantum Theory of Radiation* (Clarendon, Oxford, 1954).
- ²⁷F. Herman and S. Skillman, *Atomic Structure Calculations* (Prentice-Hall, Englewood Cliffs, N. J., 1963).
- ²⁸There are even some values of crystal fields for which we have found C^α to be negative.
- ²⁹R. Alben, J. F. Dillon, Jr., E. M. Gyorgy, and J. P. Remeika, *J. Appl. Phys.* **42**, 1447 (1971).
- ³⁰R. W. Teale, D. W. Temple, U. Enz, and R. F. Pearson, *J. Appl. Phys.* **40**, 1435 (1969).
- ³¹Broese van Groenou *et al.* considered the angular variation of the time-dependent torque and measured two quantities, which we denote A and B , related to the induced anisotropy coefficient, the speed of rotation ω , and to the relaxation time τ : $A = f(C_3 - C_2)$, $B = \omega\tau f(C_3 - C_2)$, where $f = 2\omega\tau/(1 + 4\omega^2\tau^2)$ and $C_3 - C_2$ measures the induced anisotropy coefficient (this is our G^α as defined in Table IX). In the case that differently relaxing species contribute, the measured A and B should be considered as averages \bar{A} and \bar{B} over the different τ 's. The value of $C_3 - C_2$ reported in Ref. 7 is apparently gotten from $C_3 - C_2 = [(\bar{A})^2 + 4(\bar{B})^2]/2\bar{B}$. But it may be seen that
- $$\frac{(\bar{A})^2 + 4(\bar{B})^2}{2\bar{B}} = (C_3 - C_2) \left(\frac{(\bar{A})^2 + 4(\bar{B})^2}{\langle A^2 + 4B^2 \rangle_{av}} \right).$$
- The quantity in large parentheses is clearly always less than (or equal to) unity. Thus the preceding relation for $C_3 - C_2$ is always too low. [For further discussion of aftereffect analysis, see A. H. Cook, D. T. Edmonds, C. B. P. Finn, and W. P. Wolf, *Proc. Roy. Soc. (London)* **A306**, 335 (1968).]